Deterministic Gaussian Sampling With Generalized Fibonacci Grids

Daniel Frisch and **Uwe D. Hanebeck**
Intelligent Sensor-Actuator-Systems Laboratory (ISAS)
Institute for Anthropomatics and Robotics
Karlsruhe Institute of Technology (KIT), Germany
daniel.frisch@ieee.org, uwe.hanebeck@ieee.org

***Abstract*—We propose a simple and efficient method to obtain unweighted deterministic samples of the multivariate Gaussian density. It allows to place a large number of homogeneously placed samples even in high-dimensional spaces. There is a demand for large high-quality sample sets in many nonlinear filters. The Smart Sampling Kalman Filter (S2KF), for example, uses many samples and is an extension of the Unscented Kalman Filter (UKF) that is limited due to its small sample set. Generalized Fibonacci grids have the property that if stretched or compressed along certain directions, the grid points keep approximately equal distances to all their neighbors. This can be exploited to easily obtain deterministic samples of arbitrary Gaussians. As the computational effort to generate these anisotropically scalable point sets is low, generalized Fibonacci grid sampling appears to be a great new source of large sample sets in high-quality state estimation.**

***Index Terms*—Deterministic sampling, Dirac densities, generalized Fibonacci grids, nonlinear filtering, multivariate Gaussian densities.**

I. Introduction

A. Context

We target deterministic sampling as an important building block for high-quality nonlinear state estimation and control methods.

B. Considered Problem

The focus lies on computing Fibonacci grids with arbitrary numbers of unweighted samples that approximate i) uniform densities and ii) Gaussian densities in the multivariate setting.

C. State-of-the-art

While the Kalman Filter provides exact state estimation in the linear case at low cost [1], nonlinear Gaussian filters obtain approximate Gaussian state estimations, i.e., mean and covariance, to the intractable problem of nonlinear inference. Some of them, the Linear Regression Kalman filters (LRKFs), make a *second Gaussian assumption* and estimate the covariance between state and measurement via sample sets. Most LRKFs and also truly nonlinear Gaussian filters [2], [3] need high-quality Gaussian samples as a basic building block.

The *unscented transform* exploits i) that it is easy to transform a single point by a nonlinear function, ii) it is easy to find a point cloud where mean and covariance match the moments of a given density, and iii) it is easy to obtain mean and variance of a point cloud [4]. The popular Unscented Kalman Filter (UKF) [5], [6] takes $1 + 2D$ samples for a D-dimensional state. These "sigma points" are chosen such that mean and covariance match the desired Gaussian. Said fixed number of samples is rather small. Hence, calculation is very fast, but results are often inaccurate and also inconsistent, i.e., the uncertainty is underestimated. If the function has a high degree of nonlinearity, it may be desirable to increase the number of samples and thereby accuracy and consistency.

Since is easy to obtain *univariate* deterministic Gaussian samples, one idea is to put more samples on the main axes only [7], see Fig. 2e. This is a first step, but it would be better to distribute samples in the entire space, according to the

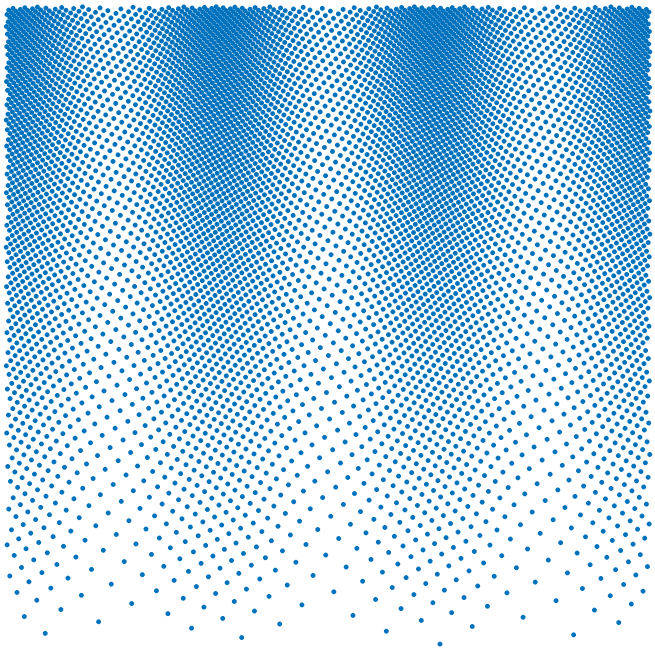

Fig. 1: Fibonacci grids can be rescaled arbitrarily along the coordinate axes without losing their "nearly-optimal sphere packing" property. Therefore, they can be transformed into stochastically independent densities particularly easily: separate the joint density into its marginals, find their inverse cumulatives, and rescale the coordinates accordingly. This figure shows 7000 samples, where the marginal densities along the x and y axis are sinusoidal and exponential, respectively.

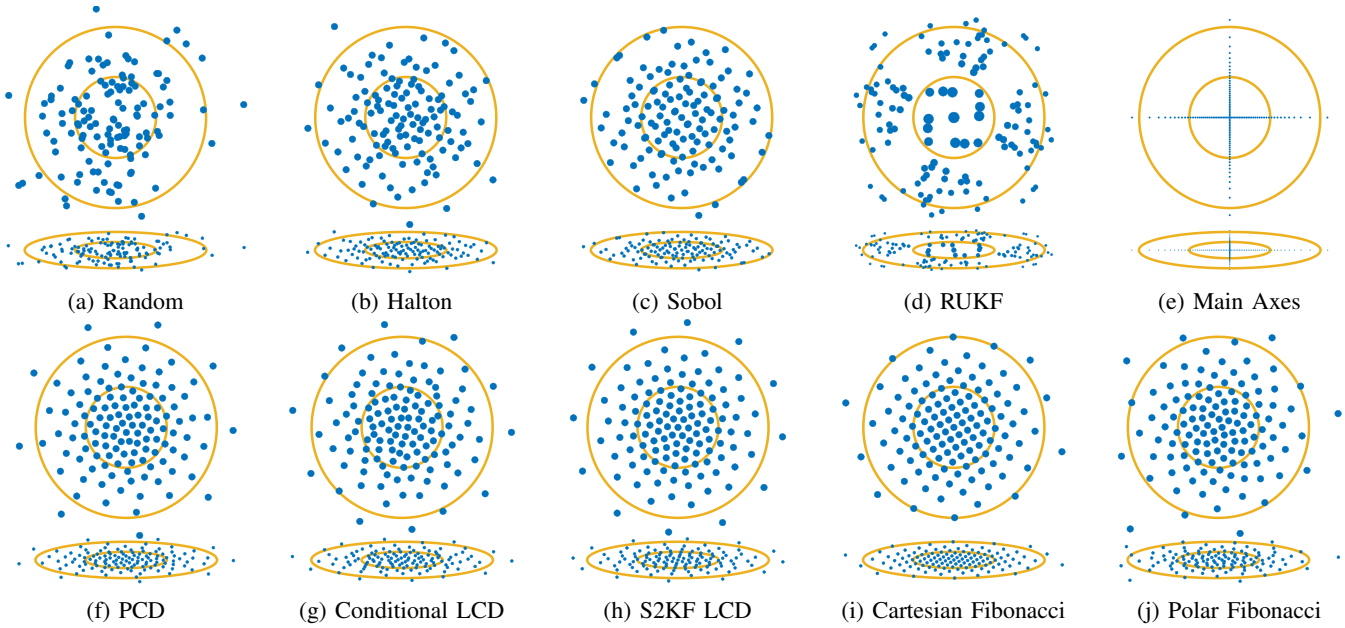

(a) Random (b) Halton (c) Sobol (d) RUKF (e) Main Axes

(f) PCD (g) Conditional LCD (h) S2KF LCD (i) Cartesian Fibonacci (j) Polar Fibonacci

Fig. 2: Comparison of various sampling methods with $L = 125$ Gaussian samples in two dimensions. Standard normal (upper parts) and scaled to $20\,\%$ along the vertical direction (lower parts). Note that the polar Fibonacci grid (j) exhibiting the conspicuous spiral pattern like a sunflower head, should be rescaled only along radial or angular direction, because scaling along y axes as shown here results in bad point discrepancy, quite different from the proposed Cartesian Fibonacci grid (i). The 1σ and 5σ bounds of the Gaussian density are indicated with yellow circles and ellipses. Note that the RUKF samples (d) are weighted as indicated by point size, all others are unweighted.

probability mass of the underlying density function, and not concentrated just on the main axes. The Randomized Unscented Kalman Filter (RUKF) exploits a degree of freedom in the UKF sampling method and creates multiple sets of sigma points, resulting in a total of $1 + 2Dq$ ($q \in \mathbb{N}$) weighted samples [8], see Fig. 2d. However, unweighted samples are preferred in order to use the available samples as efficiently as possible, especially for proposal samples or importance samples in particle filters, to avoid sample degeneracy. The Gauss-Hermite quadrature produces D^q ($q \in \mathbb{N},\ q \geq 2$) weighted samples that can also be used for filtering [9]. The cubature Kalman filters of fifth degree uses a minimum of $1 + 2D^2$ quadrature points, i.e., weighted samples [10]. All of these filters can be turned into iterative versions, where the statistical linearization is better adapted to the true posterior [11].

For obtaining an arbitrary number of unweighted samples, optimization-based methods are available that, however, require a high computational effort. The Localized Cumulative Distribution (LCD) [12] provides a distance measure that is able to compare Dirac mixture densities with continuous density functions. By minimizing this distance measure, an optimal placement of the samples is achieved, see Fig. 2h, but the numerical optimization is quite expensive, especially for higher numbers of samples. Offline calculation of *standard* normal samples stored in a sample cache allows for real-time application of LCD-based Gaussian filtering called the Smart Sampling Kalman Filter (S^2KF) [13], [14]. However, the required anisotropic linear transformation from standard to arbitrary Gaussians, by using the Cholesky decomposition of the desired covariance matrix, impedes optimality. Conditional LCD sampling can partially resolve this problem [15], see Fig. 2g.

As an alternative to the LCD, the projected cumulative distribution (PCD) yields a different and more efficient way to optimize sample locations in order to reflect a given continuous density function, see Fig. 2f. It has been demonstrated with Gaussian mixtures in the Euclidean domain $\mathbb{R}^D$ [16].

D. Challenges

So far, there is no optimization-free method for optimal or semi-optimal deterministic sampling with high (thousands) or very high (millions) numbers of samples in multi-dimensional spaces. If the system functions exhibit strong nonlinearities but are easy to evaluate, filtering quality can and should be increased by using a large number of evaluation points.

E. Fibonacci Grids

Probably the best known Fibonacci grid is the eye-catching spiral packing in polar coordinates in sunflower heads. It provides nearly equal-area packing with relatively high packing efficiency – about $70\,\%$ of that of a hexagonal close packing [17]. Arrangements of organs on plant stems or flower heads show striking spiral patterns, called phyllotaxis. Detailed studies targeting these arrangements date back more than 100 years [18]. The behavior can even be reproduced experimentally using a “magnetic cactus” [19].

The ubiquitous appearance of spiral phyllotaxis and its resilience to internal, environmental, and genetic variations, suggests a connection to mathematics [20]. And this in turn suggests that the underlying abstract concept may be generalized to higher dimensions.

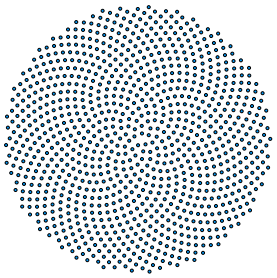

Several models have been proposed that try to explain the biological processes in the meristem that create the spiral phyllotaxis, e.g., the Hofmeister hypothesis and Snow hypothesis [21]. Investigations on a molecular level in plants showed the plant hormone auxin is triggering the organ initiation. This activator is then consumed by the growing organ, effectively inhibiting the initiation of an adjacent organ [20]. In summary, opportunistic organ initiation constitutes an entirely local mechanism and explains phyllotaxis, just as stated in the Hofmeister hypothesis [20]. The occurrence of spirals and the golden angle as divergence angle is therefore probably an emergent by-product rather than the mechanistic principle of the morphogenetic process [20].

The Fibonacci grid is presented as cubature point set with low discrepancy for quasi-Monte Carlo (QMC) integration in $\mathbb{R}^2$, generated via a lattice rule, in [22], [23]. A two-dimensional "golden set" that is a slightly irregular variant of the Fibonacci grid is introduced in [24]. The irregularity avoids aliasing in Monte Carlo integrations for ray tracing. The authors also demonstrate the flexibility of the golden set by transforming it into Cartesian coordinates. They also warp it into a bivariate Gaussian mixture. There is also a broad literature about irregular but low-discrepancy point sets like the Halton, Hammersley, and Sobol sequence [25], [26], or based on Fibonacci polynomials [27].

Some interesting and fundamental aspects regarding Fibonacci grids have been researched by meteorologists, in order to obtain spherical grids for global weather prediction [28]. The "sunflower Fibonacci grid" in polar coordinates can be represented in a Cartesian, cylindrical, or spherical coordinate system with suitable projections such as the Lambert equal-area cylindrical projection of the globe. In Cartesian notation, it is possible to introduce basis vectors that span the grid points and this way investigate the properties of the grid. Formal proofs regarding bounds of the minimum point distance and Voronoi cell properties of two-dimensional Fibonacci lattices and grids are given in [29]. It also shows how existing Fibonacci grids can be subsequently refined while keeping the original points.

The main reference this work is based on is Purser's generalization of the well-known two-dimensional Fibonacci grid to higher dimensions [30]. It states that the "orthogonal orientations of the eigenvectors of the Fibonacci matrix provide the optimal choice for principal component directions of pure deformations when it is required that the action of arbitrary deformations of this kind lead to no close collisions of the deformed lattice points" [30, p. 2]. It then focuses mainly on the construction of a three-dimensional generalized Fibonacci grid and the properties of the corresponding system of generalized Fibonacci numbers.

F. Key Idea

We propose to generate uniform Fibonacci grids in higher dimensions on the $(0,1)^D$ domain, and from there transform them to arbitrary Gaussian densities. By doing so, we take care to rescale the grid only along the "allowed directions". Hence, the points maintain a homogeneous distribution. This is an inherent property of Fibonacci grids, see Fig. 1 for a visual example. Therefore, we can treat the samples individually and do not need to consider any neighborhood relations or to calculate distances between adjacent samples. This is the reason for our method being extremely efficient.

II. Problem Formulation

A Dirac mixture

$$^{\mathrm{DM}}f(\underline{x}) = \frac{1}{L}\sum_{i=1}^{L}\underline{x}_i$$

with sample locations

$$\underline{x}_i = \begin{bmatrix} x_i^{(1)} & x_i^{(2)} & \dots & x_i^{(D)} \end{bmatrix}^\top \in \mathbb{R}^D$$

should be found such that it approximates a given Gaussian reference density

$$\begin{aligned}\tilde{f}(\underline{x}) &= \mathcal{N}\left(\underline{x};\underline{\mu},\mathbf{C}\right)\\ &= \frac{1}{\sqrt{|2\pi\mathbf{C}|}}\exp\left(-\frac{1}{2}\left(\underline{x}-\underline{\mu}\right)^\top\mathbf{C}^{-1}\left(\underline{x}-\underline{\mu}\right)\right)\end{aligned}$$

with arbitrary mean vector $\underline{\mu}\in\mathbb{R}^D$ and symmetric positive semidefinite covariance matrix $\mathbf{C}\in\mathbb{R}^{D\times D}$.

Input and Output

Our method provides deterministic samples of normal densities in real time. Required inputs are

- I1 the number L of wanted samples,
- I2 the dimension D, with $(2D+1)$ prime [30]
- I3 optionally, covariance matrix $\mathbf{C}$,
- I4 optionally, mean vector $\underline{\mu}$.

From these, we compute a deterministic set of particles that approximates the Gaussian density with the specified parameters.

III. Method Derivation

In this section, we show how the Fibonacci grid can be generalized to dimensions larger than two, yielding a uniformly distributed, anisotropically scalable sample set. In a second step, a suitable transformation then turns that point set into a deterministic approximation of any Gaussian density.

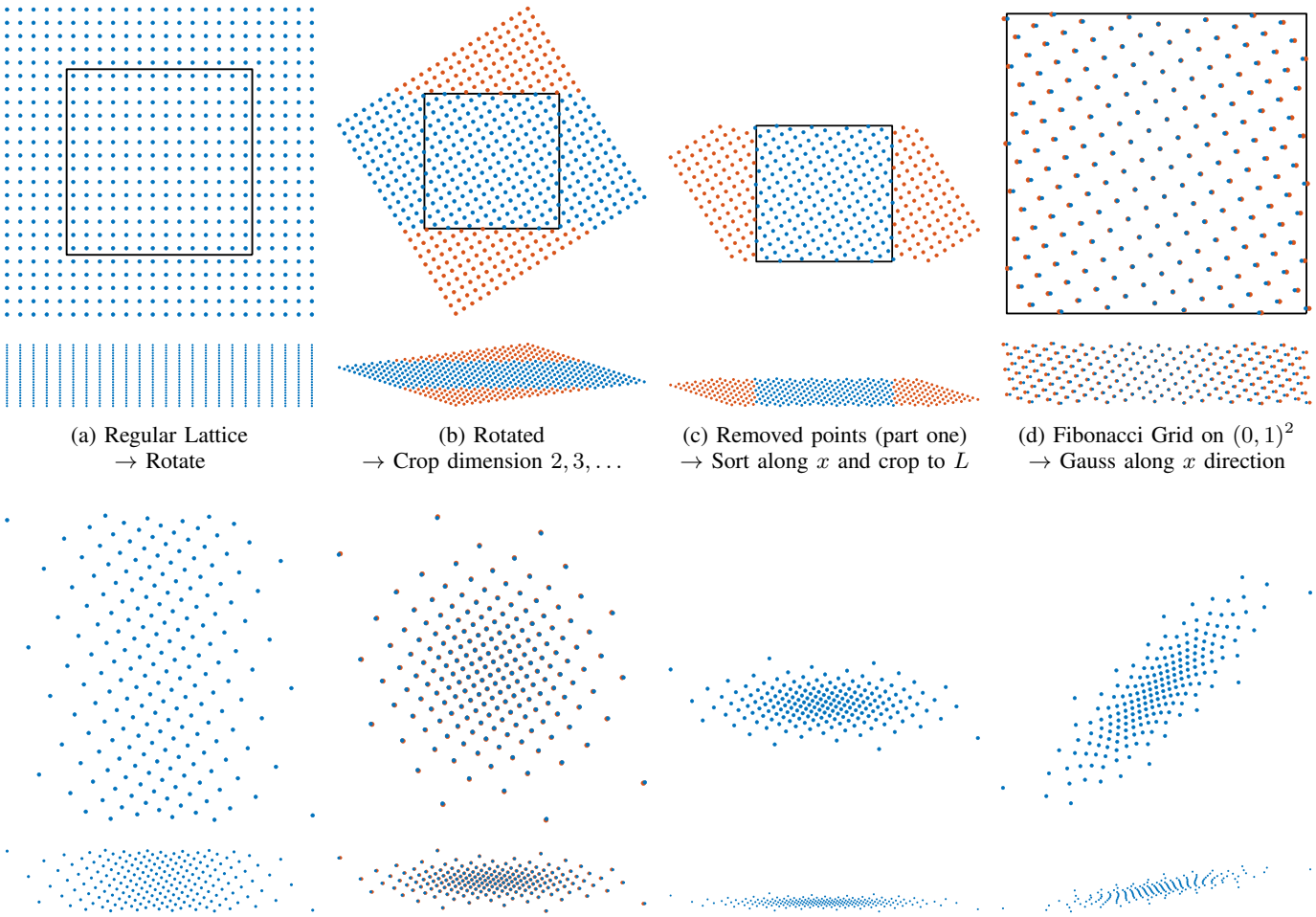

(a) Regular Lattice
→ Rotate

(b) Rotated
→ Crop dimension $2, 3, \ldots$

(c) Removed points (part one)
→ Sort along x and crop to L

(d) Fibonacci Grid on $(0, 1)^2$
→ Gauss along x direction

(e) Gaussian along x direction
→ Gauss along y direction

(f) Standard Normal
→ Anisotropic Rescale

(g) Uncorrelated Gaussian
→ Rotate

(h) Arbitrary Gaussian
→ Use in filter

Fig. 3: Step by step procedure to generate arbitrary Gaussian sample sets using Fibonacci grids. Refer to Alg. 1 and the source code for more details. Red and blue point duplicates in (d, f) denote a slight rescaling by a diagonal matrix for correction purposes. A vertically compressed version is plotted under each figure purely to demonstrate the effects of anisotropic rescaling. Note the difference when applying this rescaling along an "allowed" direction (lower part of: b, c, d, e, f, g), versus some different direction (lower part of: a, h).

A. *Fibonacci Matrix*

The D-dimensional Fibonacci matrix $\mathbf{M}_D$ is defined as

$$[\mathbf{M}_D]_{i,j} = \begin{cases} 1, & i + j \leq D + 1 \\ 0, & i + j > D + 1 \end{cases} ,$$

for example,

$$\mathbf{M}_2 = \begin{bmatrix} 1 & 1 \\ 1 & 0 \end{bmatrix} , \qquad \mathbf{M}_3 = \begin{bmatrix} 1 & 1 & 1 \\ 1 & 1 & 0 \\ 1 & 0 & 0 \end{bmatrix} .$$

The eigenvalue decomposition

$$\mathbf{M}_D = \mathbf{V}_D \, \mathbf{D}_D \mathbf{V}_D^\top ,$$

splits $\mathbf{M}_D$ into unitary $\mathbf{V}_D$ and diagonal $\mathbf{D}_D$. The eigenvectors $\mathbf{V}_D$ can be obtained by properly normalizing the unnormalized eigenvector matrix $\mathbf{V}_D^{\mathrm{u}}$ which is given by [30]

$$[\mathbf{V}_D^{\mathrm{u}}]_{i,j} = \cos\left(\frac{(2i-1)\,(2j-1)\,\pi}{4D+2} \right) . \tag{1}$$

B. *Generalized Fibonacci Grid*

We start with generating a generalized Fibonacci grid that resembles a uniform density with L grid points on the domain $(0, 1)^D$. A regular grid in the Euclidean domain can be anisotropically compressed or stretched along the eigenvectors of the Fibonacci matrix with no close collisions [30]. Therefore, one conceptually easy way generating a generalized Fibonacci grid is to create a regular grid and rotate it such that said "allowed" deformation axes are aligned with the standard basis.

Let $\mathbf{X}_{\mathrm{reg}} \in \mathbb{R}^{D \times L_{\mathrm{reg}}}$ be a matrix containing points $\underline{x}_i \in \mathbb{R}^D$ of a regular grid

$$\mathbf{X}_{\mathrm{reg}} = \begin{bmatrix} \underline{x}_1 & \underline{x}_2 & \dots & \underline{x}_{L_{\mathrm{reg}}} \end{bmatrix} \ ,$$
$$\underline{x}_i = \sum_{d=1}^{D} b_{d,i}\, \alpha\, \underline{e}_d \,, \quad b_{d,i} \in \mathbb{Z} \,, \quad \alpha \in \mathbb{R}_+ \,,$$

where α denotes the spacing of the grid, and $b_{d,i}$ are all the indices where the grid is in the desired region, see Fig. 3a for an example. A suitable rotation matrix that aligns the allowed rotation directions with the standard basis is $\mathbf{V}_D^\top$ (1). We obtain $\mathbf{X}_{\mathrm{rot}} \in \mathbb{R}^{D \times L_{\mathrm{reg}}}$

$$\mathbf{X}_{\mathrm{rot}} = \mathbf{V}_D^\top \mathbf{X}_{\mathrm{reg}} \ ,$$

a "Fibonacci template" that still has to be cut to the wanted size. Anisotropic scaling is now "allowed" along the standard basis, i.e., $\mathbf{X}_{\mathrm{rot}}$ can be transformed using any diagonal matrix while keeping its good sphere packing properties. It is easy to find a combination of such scaling and removing some samples until we obtain exactly L samples $\mathbf{X}_{\mathrm{Fib}} \in \mathbb{R}^{D \times L}$

$$\mathbf{X}_{\mathrm{Fib}} = \begin{bmatrix} \underline{x}_1 & \underline{x}_2 & \dots & \underline{x}_L \end{bmatrix}$$

that uniformly cover the domain $(0,1)^D$. Refer to Alg. 1, the source code, and also Fig. 3 (b, c, d) for more details.

C. Standard Normal Gaussian

Scaling along the "allowed" directions in a Fibonacci grid can be performed not only with constant factors, but also with functions that vary along those directions. This is demonstrated in Fig. 1. We exploit this to transform the uniformly distributed samples $\mathbf{X}_{\mathrm{Fib}}$ into standard normally distributed samples.

The one-dimensional standard normal density $f(x)$, its cumulative density function (CDF) $F(x)$, and the inverse CDF $F^{-1}(p)$ are given by

$$f(x) = \frac{1}{\sqrt{2\pi}} \exp\left(-\frac{1}{2}x^2\right) \ ,$$
$$F(x) = \frac{1}{2}\left(1 + \mathrm{erf}\left(\frac{x}{\sqrt{2}}\right)\right) \ ,$$
$$F^{-1}(p) = \sqrt{2} \cdot \mathrm{erf}^{-1}(2p-1) \ , \tag{2}$$

where $\mathrm{erf}(x)$ is the error function

$$\mathrm{erf}(x) = \frac{2}{\sqrt{\pi}} \int_0^x \exp\left(-t^2\right) \mathrm{d}t \ .$$

Therefore, uniform samples in $(0,1)^D$ can be transformed to standard normally distributed samples in $\mathbb{R}^D$ by propagating them through the inverse CDF (2)

$$[\mathbf{X}_{\mathrm{Std}}]_{d,i} = \sqrt{2} \cdot \mathrm{erf}^{-1}(2 \cdot [\mathbf{X}_{\mathrm{Fib}}]_{d,i} - 1) \ . \tag{3}$$

This transformation is also used to create standard normally distributed random numbers from uniform random numbers.

It is beneficial to perform a moment correction at this point. We are "allowed" to compress or stretch the now Gaussian particle cloud along the standard basis vectors, and we can use this to match the diagonal components of the covariance matrix, i.e., the sample variances along the coordinate axes, exactly to unity. First, we determine said diagonal components

$$\nu_d = \frac{1}{L} \sum_{i=1}^{L} [\mathbf{X}_{\mathrm{Std}}]_{d,i}^2$$

and rescale the Gaussian samples slightly to be more accurate

$$[\mathbf{X}_{\mathrm{StdMM}}]_{d,i} = \frac{[\mathbf{X}_{\mathrm{Std}}]_{d,i}}{\sqrt{\nu_d}} \ .$$

Algorithm 1: Uniform Fibonacci grid sampling. See Fig. 3 for visualizations of the intermediate steps.

Function $\{\underline{x}_{\mathrm{Fib},i}\}_{i=1}^{L} \leftarrow$ `fibonacci_grid(`D, L`)`
Input: D: dimension,
L: number of samples
Output: $\{\underline{x}_i\}_{i=1}^{L}$: unweighted samples
`// Fibonacci matrix eigenvectors (1)`
$\mathbf{V}_D \leftarrow$ `fib_eigen(`D`)`
`// Smallest hyperrectangle`
$\underline{s} \leftarrow \left\{\sum_{j=1}^{D} \left|[\mathbf{V}_D]_{d,j}\right|\right\}_{d=1}^{D}$
`// Smallest hypercube`
$s_{\mathrm{HC}} \leftarrow \max_d \{|s^{(d)}|\}$
`// Create sampling vector` $\underline{r}$
$L_0 \leftarrow \left\lceil \sqrt[D]{L} \right\rceil$
$\delta \leftarrow 1/L_0$
$L_1 \leftarrow \lceil s_{\mathrm{HC}}/\delta \rceil$
$L_1 \leftarrow L_1 + 2$ `// some extra border`
if $\mathrm{mod}(L,2) \neq \mathrm{mod}(L_1,2)$ **then**
  $L_1 \leftarrow L_1 + 1$ `// point in origin?`
$\underline{r} \leftarrow \{j \cdot \delta\}_{j=1}^{L_1}$ `// 1D sampling vector`
$\underline{r} \leftarrow \underline{r} - \frac{1}{L_1} \cdot \underline{r}^\top \cdot \underline{1}$ `// centering`
`// Create grid with` L_1^D `points`
$\mathbf{X}_{\mathrm{reg}} \leftarrow$ `ndgrid(`D, $\underline{r}$`)` `// (`$D \times L_1^D$`) reg. grid`
$\mathbf{X}_{\mathrm{rot}} \leftarrow \mathbf{V}_D^\top \cdot \mathbf{X}_{\mathrm{reg}}$ `// rotate`
`// Remove unwanted points, 1st round`
$\{\underline{x}_{\mathrm{Fib},i}\}_{i=1}^{L_2} \leftarrow \left\{\underline{x}_{\mathrm{rot},i} \;\middle|\; \bigcap_{d=2}^{D} x_{\mathrm{rot},i}^{(d)} \in \left[-\frac{1}{2}, \frac{1}{2}\right]\right\}$
`// Sort by 1st coordinate`
$\pi \leftarrow$ `sort_ind(`$\left\{x_{\mathrm{Fib},i}^{(1)}\right\}_{i=1}^{L_2}$`)`
$\{\underline{x}_{\mathrm{Fib},i}\}_{i=1}^{L_2} \leftarrow \left\{\underline{x}_{\mathrm{Fib},\pi(i)}\right\}_{i=1}^{L_2}$
`// Remove points, 2nd round (simplified)`
$u \leftarrow (L_2 - L)/2$
$\{\underline{x}_{\mathrm{Fib},i}\}_{i=1}^{L} \leftarrow \{\underline{x}_{\mathrm{Fib},i}\}_{i=u+1}^{L_2-u}$
`// Rescaling for wanted border`
$b \leftarrow \frac{1}{2} - \frac{1}{2L}$ `// wanted border`
$\underline{m} \leftarrow \left\{\max_i \left\{x_{\mathrm{Fib},i}^{(d)}\right\}\right\}_{d=1}^{D}$ `// current border`
$\{\underline{x}_{\mathrm{Fib},i}\}_{i=1}^{L} \leftarrow \{\underline{x}_{\mathrm{Fib},i} \oslash \underline{m} \cdot b\}_{i=1}^{L}$ `// equalize`
`// From` $\left(-\frac{1}{2}, \frac{1}{2}\right)^D$ `to` $(0,1)^D$
$\{\underline{x}_{\mathrm{Fib},i}\}_{i=1}^{L} \leftarrow \{\underline{x}_{\mathrm{Fib},i} + \underline{1} \cdot \frac{1}{2}\}_{i=1}^{L}$

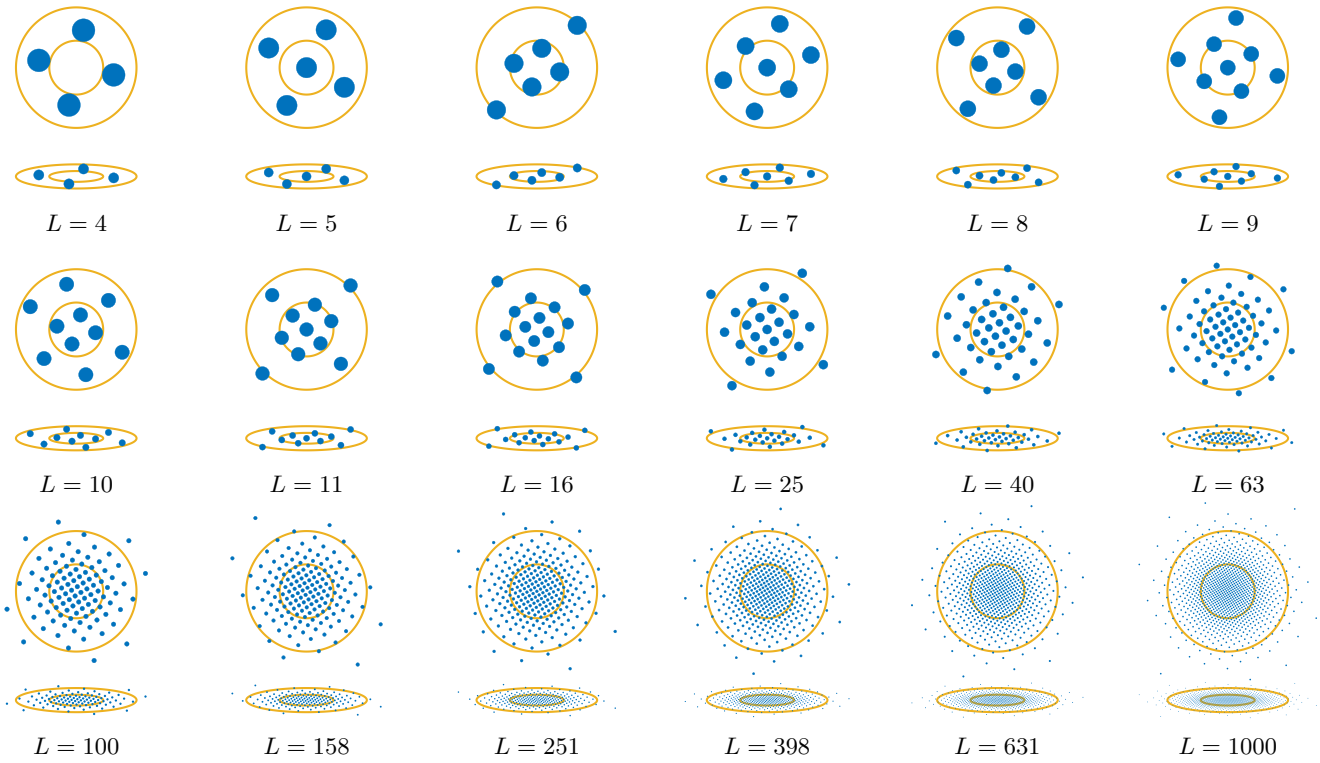

Fig. 4: Examples of deterministic sample approximations of the two-dimensional standard normal distribution, with anisotropic scaling below (factor 0.2 along y direction). One-σ-bounds and five-σ-bounds are marked as yellow circles and ellipses. Planar examples are shown for easier visualization. The method however works also in higher dimensions where $2D + 1$ is prime.

Note that the mean of the samples is already $\underline{0}$ if we place them in a symmetric manner.

In this section, we described how to obtain standard normal samples from uniform Fibonacci samples using Gaussian inverse CDF transform sampling. See Fig. 3e, where the transform is applied only along the x axis, for $d = 1$ in (3). Fig. 3f shows the standard normal Gaussians $\mathbf{X}_{\mathrm{Std}}$ and $\mathbf{X}_{\mathrm{StdMM}}$ in red and blue, respectively. Fig. 4 visualizes $\mathbf{X}_{\mathrm{StdMM}}$ for many different numbers of samples $L \in [4, 1000]$.

D. Arbitrary Gaussians

The set of samples $\mathbf{X}_{\mathrm{StdMM}}$ that approximates a standard normal density can now easily be transformed into an arbitrary Gaussian density, e.g., a Gaussian density with an arbitrary sample variance along each dimension and an arbitrary correlation coefficient for each pair of dimensions. Thereby the sample set retains its optimality regarding the homogeneous distribution of points. Although the Cholesky decomposition $\mathbf{L}$ of a covariance matrix $\mathbf{C} = \mathbf{L}\mathbf{L}^\top$ is often used to transform standard normally distributed samples into arbitrary Gaussian densities, we must again make sure that any anisotropic scaling takes effect along the "allowed" directions only. Therefore, we need the eigenvalue and eigenvector decomposition $\mathbf{V}\mathbf{D}\mathbf{V}^\top = \mathbf{C}$, with $\mathbf{V}$ unitary and $\mathbf{D}$ diagonal. The final sample set $\mathbf{X}_{\mathrm{Gauss}}$ is then given by

$$\mathbf{X}_{\mathrm{Gauss}} = \mathbf{V}\,\mathbf{D}\,\mathbf{X}_{\mathrm{Std}} + \underline{\mu} \ . \tag{4}$$

If $\mathbf{C}$ is not positive definite but positive semidefinite and thus singular with rank $D_{\mathrm{R}} = D - D_{\mathrm{S}}$, then first generate a D_{R}-dimensional standard normal template $\mathbf{X}_{\mathrm{Std,R}}$, insert rows of arbitrary values, e.g., zeros, where $\mathbf{D}$ has zeros on its diagonal, and use the resulting point set as $\mathbf{X}_{\mathrm{Std}}$ in (4).

IV. Evaluation

For evaluation, we estimate the expectation value of

$$y = g(\underline{x}) = \|\underline{x}\|_2 = \sqrt{\left(x^{(1)}\right)^2 + \left(x^{(2)}\right)^2 + \left(x^{(3)}\right)^2} \ ,$$

where $\underline{x}$ is a three-dimensional zero-mean Gaussian vector with standard deviations 5, 1, and 2 along the main axes, tilted by a random direction in $\mathrm{SO}(3)$. Sample sets $\mathbf{X}_{\mathrm{Gauss}} \in \mathbb{R}^{3\times L}$ of different size L and from various sampling methods are propagated through $g(\cdot)$ and the statistics of the resulting estimate are calculated. Estimation results and computation times are shown in Fig. 5.

Random Gaussian samples are the easiest and fastest to obtain as they are produced independently. However, in our example, comparable results can be achieved with less than one hundredth of the samples using deterministic sampling.

The deterministic sampling method used in the S^{2}KF obtains symmetric samples by minimizing a distance measure that is based on the LCD, thereby minimizing the distance between the sample set and the standard normal density function [13]. It

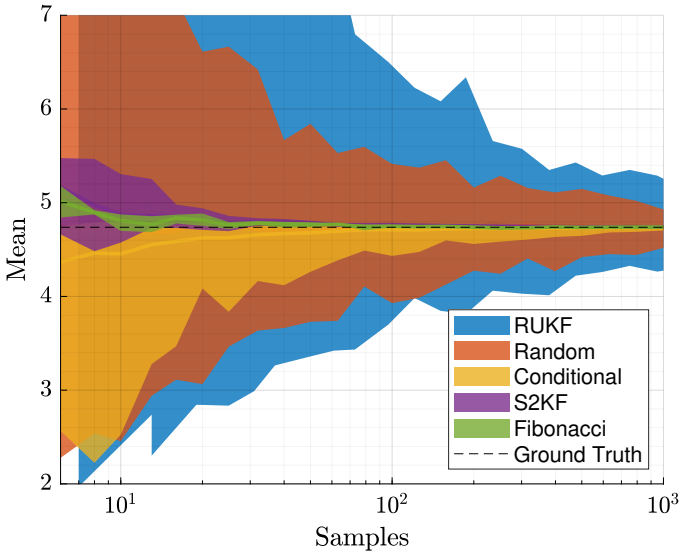

(a) Mean Estimation

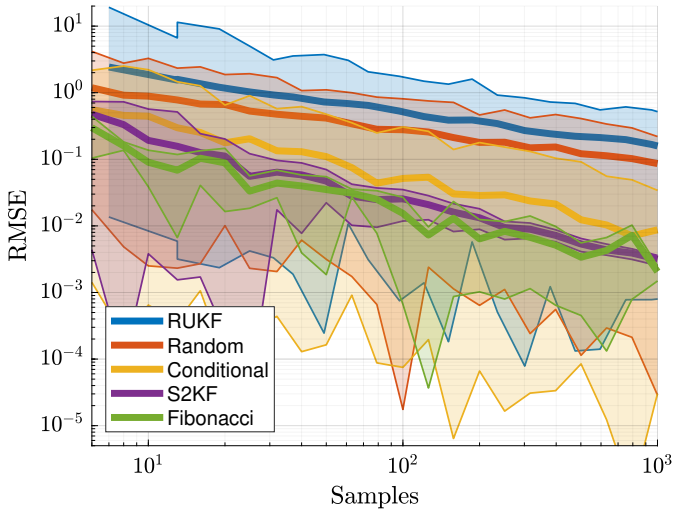

(b) Mean Error

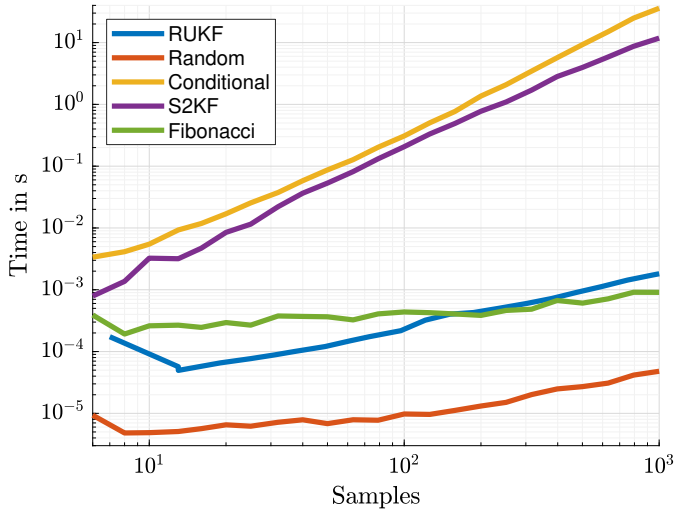

(c) Calculation Time

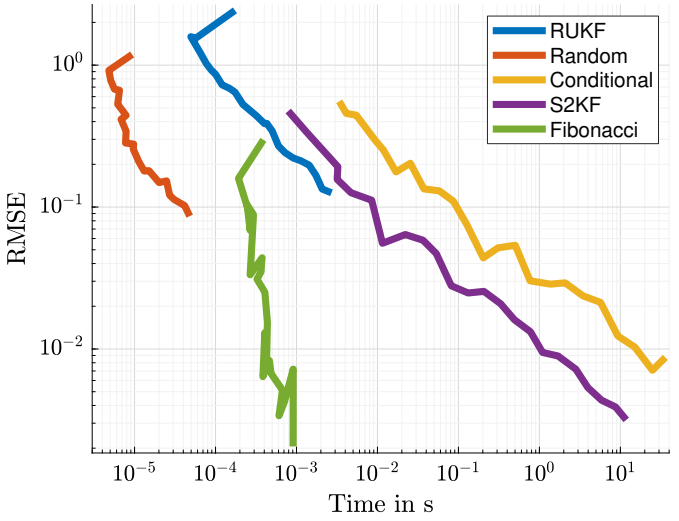

(d) Pareto Diagram

Fig. 5: Evaluation of sampling methods by nonlinear moment estimation in a three-dimensional setting. In (a), the minimum and maximum value and in (b), the best and worst result out of 200 trials is indicated by the shaded area. Solid lines show the mean of all trials. Note that the S^{2}KF and conditional samples are usually generated offline and stored in a library. Calculation times in (c, d) denote the effort to generate the samples for the library.

then uses the Cholesky decomposition to transform the standard Gaussian samples into arbitrary Gaussian ones, therefore there is an undefined rotational component. The resulting range of possible results is indicated in Fig. 5 (a, b).

Conditional sampling is a variant of S^{2}KF sampling. When generating the standard normal samples, it already takes into account the subsequent compression along certain directions that is required to obtain arbitrary Gaussians [15]. The transformation is uniquely defined by the eigenvalues and eigenvectors of the covariance matrix. However, repeated sample calculation of the samples (without using sample cache) leads to different local minima and thus to a range of possible results that is again shown in Fig. 5. The results vary vastly which indicates that multiple optimization attempts should be done when creating the offline library in order to avoid local optima.

For Fibonacci sampling as proposed in this work, the transformation (4) from standard normal (3) to arbitrary Gaussian samples, visualized in Fig. 3 (f, g, h), is defined uniquely up to a permutation of the eigenvectors and eigenvalues of the desired covariance matrix. The range of possible results is again indicated as shaded area in Fig. 5 (a, b).

V. Conclusions

A new method for generating large sample sets for approximating Gaussian densities in high-dimensional spaces has been developed. The samples are equally weighted, placed homogeneously, and have nice statistical properties. A huge

advantage over other deterministic sampling schemes is that the samples can be arbitrarily and anisotropically scaled. In addition, in two dimensions, the results are aesthetically pleasing.

The sampling method is easy to implement with the recipe given in this paper. As no optimization is required, the method is fast and can easily generate millions of samples. It is especially well suited for large sample sets as appropriate methods for small and medium size sets are readily available. Hence, the method is especially useful when a high sample resolution is required and the evaluation of samples is inexpensive.

Matlab source code of the presented uniform and Gaussian sampling is provided in IEEE Xplore alongside this paper. State of the art sampling methods like RUKF and S^2KF have been produced using the nonlinear estimation toolbox [31].

VI. Future Work

The next step is to generalize the method for sampling Gaussian densities as described in this paper to more complex densities such as Gaussian mixture densities. This is possible with generalizing the nonlinear scaling from subsection III-C.

Generating uniform Fibonacci grids via the proposed rotation of an extended regular grid and subsequent rejection is conceptually simple and easy to implement. However, it entails discarding the unused points outside the unit cube, which is wasting memory or computation time, especially in higher dimensions. Therefore, we will develop an implementation that directly places the points inside the unit square at the appropriate locations. Furthermore, we will improve moment matching: in the present work, only the diagonal entries of the covariance matrix $\mathbf{X}_{\mathrm{StdMM}}$ are matched, while the correlation coefficients are slightly non-zero.

In analogy to the sunflower pattern in polar coordinates, which is periodic in the angular component, a generalization to sample approximations of hyperspherical densities will be performed similar to the generalization performed in this paper.

References

[1] R. E. Kalman, "A New Approach to Linear Filtering and Prediction Problems," *Journal of Basic Engineering*, vol. 82, no. 1, pp. 35–45, Mar. 1960.

[2] U. D. Hanebeck, "PGF 42: Progressive Gaussian Filtering with a Twist," in *Proceedings of the 16th International Conference on Information Fusion (Fusion 2013)*, Istanbul, Turkey, Jul. 2013.

[3] D. Frisch and U. D. Hanebeck, "Progressive Bayesian Filtering with Coupled Gaussian and Dirac Mixtures," in *Proceedings of the 23rd International Conference on Information Fusion (Fusion 2020)*, Virtual, Jul. 2020.

[4] D. Simon, "The Unscented Kalman Filter," in *Optimal State Estimation*. John Wiley & Sons, Ltd, 2006, pp. 433–459.

[5] S. J. Julier, "The Scaled Unscented Transformation," in *Proceedings of the 2002 American Control Conference (IEEE Cat. No.CH37301)*, vol. 6, May 2002, pp. 4555–4559 vol.6.

[6] S. J. Julier and J. K. Uhlmann, "New Extension of the Kalman Filter to Nonlinear Systems," in *Signal Processing, Sensor Fusion, and Target Recognition VI*, vol. 3068. International Society for Optics and Photonics, Jul. 1997, pp. 182–193.

[8] J. Duník, O. Straka, and M. Simandl, "The Development of a Randomised Unscented Kalman Filter," *IFAC Proceedings Volumes*, vol. 44, no. 1, pp. 8–13, 2011, 18th IFAC World Congress.

[7] M. F. Huber and U. D. Hanebeck, "Gaussian Filter based on Deterministic Sampling for High Quality Nonlinear Estimation," in *Proceedings of the 17th IFAC World Congress (IFAC 2008)*, vol. 17, no. 2, Seoul, Republic of Korea, Jul. 2008.

[9] K. Ito and K. Xiong, "Gaussian Filters for Nonlinear Filtering Problems," *IEEE Transactions on Automatic Control*, vol. 45, no. 5, pp. 910–927, 2000.

[10] B. Jia, M. Xin, and Y. Cheng, "High-Degree Cubature Kalman Filter," *Automatica*, vol. 49, no. 2, pp. 510–518, 2013.

[11] Á. F. García-Fernández, L. Svensson, M. R. Morelande, and S. Särkkä, "Posterior Linearization Filter: Principles and Implementation Using Sigma Points," *IEEE Transactions on Signal Processing*, vol. 63, no. 20, pp. 5561–5573, 2015.

[12] U. D. Hanebeck and V. Klumpp, "Localized Cumulative Distributions and a Multivariate Generalization of the Cramér-von Mises Distance," in *Proceedings of the 2008 IEEE International Conference on Multisensor Fusion and Integration for Intelligent Systems (MFI 2008)*, Seoul, Republic of Korea, Aug. 2008, pp. 33–39.

[13] J. Steinbring and U. D. Hanebeck, "LRKF Revisited: The Smart Sampling Kalman Filter (S2KF)," *Journal of Advances in Information Fusion*, vol. 9, no. 2, pp. 106–123, Dec. 2014. [Online]. Available: https://confcats_isif.s3.amazonaws.com/web-files/journals/entries/441_1_art_11_17020.pdf

[14] J. Steinbring, M. Pander, and U. D. Hanebeck, "The Smart Sampling Kalman Filter with Symmetric Samples," *Journal of Advances in Information Fusion*, vol. 11, no. 1, pp. 71–90, Jun. 2016.

[15] D. Frisch and U. D. Hanebeck, "Efficient Deterministic Conditional Sampling of Multivariate Gaussian Densities," in *Proceedings of the 2020 IEEE International Conference on Multisensor Fusion and Integration for Intelligent Systems (MFI 2020)*, Virtual, Sep. 2020.

[16] U. D. Hanebeck, "Deterministic Sampling of Multivariate Densities based on Projected Cumulative Distributions," in *Proceedings of the 54th Annual Conference on Information Sciences and Systems (CISS 2020)*, Princeton, New Jersey, USA, Mar. 2020.

[17] J. Ridley, "Packing Efficiency in Sunflower Heads," *Mathematical Biosciences*, vol. 58, no. 1, pp. 129–139, 1982.

[18] G. v. G. Iterson, *Mathematische und mikroskopisch-anatomische Studien über Blattstellungen nebst Betrachtungen über den Schalenbau der Miliolinen.* Jena: Fischer, 1907.

[19] C. Nisoli, N. M. Gabor, P. E. Lammert, J. D. Maynard, and V. H. Crespi, "Annealing a Magnetic Cactus Into Phyllotaxis," *Phys. Rev. E*, vol. 81, p. 046107, Apr 2010.

[20] C. Godin, C. Golé, and S. Douady, "Phyllotaxis as Geometric Canalization During Plant Development," *Development*, vol. 147, no. 19, 10 2020.

[21] S. Hotton, V. Johnson, J. Wilbarger, K. Zwieniecki, P. Atela, C. Golé, and J. Dumais, "The Possible and the Actual in Phyllotaxis: Bridging the Gap between Empirical Observations and Iterative Models," *Journal of Plant Growth Regulation*, vol. 25, no. 4, pp. 313–323, Dec 2006.

[22] J. Dick, F. Y. Kuo, and I. H. Sloan, "High-Dimensional Integration: The Quasi-Monte Carlo Way," *Acta Numerica*, vol. 22, p. 133–288, 2013.

[23] L. N. Trefethen, "Cubature, Approximation, and Isotropy in the Hypercube," *SIAM Review*, vol. 59, no. 3, pp. 469–491, 2017.

[24] C. Schretter, L. Kobbelt, and P.-O. Dehaye, "Golden Ratio Sequences for Low-Discrepancy Sampling," *Journal of Graphics Tools*, vol. 16, no. 2, pp. 95–104, 2012.

[25] T.-T. Wong, W.-S. Luk, and P.-A. Heng, "Sampling with Hammersley and Halton Points," *Journal of Graphics Tools*, vol. 2, no. 2, pp. 9–24, 1997.

[26] S. S. Garud, I. A. Karimi, and M. Kraft, "Design of Computer Experiments: A Review," *Computers & Chemical Engineering*, vol. 106, pp. 71–95, 2017, eSCAPE-26.

[27] S. Tezuka and M. Fushimi, "Fast Generation of Low Discrepancy Points Based on Fibonacci Polynomials," in *Proceedings of the 24th Conference on Winter Simulation*, ser. WSC '92. New York, NY, USA: Association for Computing Machinery, 1992, p. 433–437.

[28] R. Swinbank and R. James Purser, "Fibonacci Grids: A Novel Approach to Global Modelling," *Quarterly Journal of the Royal Meteorological Society*, vol. 132, no. 619, pp. 1769–1793, 2006.

[29] R. Marques, C. Bouville, K. Bouatouch, and J. Blat, "Extensible Spherical Fibonacci Grids," *IEEE Transactions on Visualization and Computer Graphics*, vol. 27, no. 4, pp. 2341–2354, 2021.

[30] R. J. Purser, "Generalized Fibonacci Grids; A New Class of Structured, Smoothly Adaptive Multi-Dimensional Computational Lattices," *Office note (National Centers for Environmental Prediction (U.S.))*, 2008.

[31] J. Steinbring, "Nonlinear Estimation Toolbox." [Online]. Available: https://bitbucket.org/nonlinearestimation/toolbox